

Superresolution imaging of scatterers in ultrasound B-scan imaging

Kevin J. Parker^{a)}

Department of Electrical and Computer Engineering, University of Rochester, Hopeman Engineering Building 203, P.O. Box 270126, Rochester, New York 14627-0126

(Received 12 December 2011; revised 16 April 2012; accepted 17 April 2012)

A number of imaging systems exhibit speckle, which is caused by the interaction of a coherent pulse reflecting off of random reflectors. The limitations of these systems are quite serious because the speckle phenomenon creates a pattern of nulls and peaks from subresolvable scatterers or targets that are difficult to interpret. Another limitation of these pulse-echo imaging systems is that their resolution is dependent on the full spatial extent of the propagating pulse, usually several wavelengths in the axial or propagating dimension and typically longer in the transverse direction. This limits the spatial resolution to many multiples of the wavelength. This paper focuses on the particular case of ultrasound B-scan imaging and develops an inverse filter solution that eliminates both the speckle phenomenon and the poor resolution dependency on the pulse length and width to produce super-resolution ultrasound (SURUS) images. The key to the inverse filter is the creation of pulse shapes that have stable inverses. This is derived by use of the standard Z-transform and related properties. Although the focus of this paper is on examples from ultrasound imaging systems, the results are applicable to other pulse-echo imaging systems that also can exhibit speckle statistics.

© 2012 Acoustical Society of America. [<http://dx.doi.org/10.1121/1.4714341>]

PACS number(s): 43.60.Pt [PEB]

Pages: 4680–4689

I. INTRODUCTION

At the heart of analytical models of pulse-echo imaging is an integration on the product of the propagating pulse and the reflectors or scatterers, over the location of the pulse at some point in time (Macovski, 1983; Szabo, 2004; Prince and Links, 2006). Under a number of approximations and simplifications about attenuation and diffraction, the integration can be reduced to a convolution model (Macovski, 1983) such that the received echo $e(t)$ is approximated by

$$e(t) = A \left\{ p(t) s(x, y) * * * R \left(x, y, \frac{ct}{2} \right) \right\} \quad (1)$$

where A is an amplitude constant, $p(t)$ is the propagating pulse in the axial direction, $s(x, y)$ is the beam width in the transverse and elevational axes (and thus the beam pattern is assumed to be a separable function), and $R(x, y, z)$ is the three-dimensional (3D) pattern of reflectors or scatterers. The speed of sound is c , and with a round trip for the echo, the axial distance z is replaced by $ct/2$ in the 3D convolution represented by the symbol $* * *$. The problems of poor resolution and speckle can be understood as a direct result of this convolution. The spatial resolution is set by the full spatial extent of the propagating pulse in 3D that is typically many multiples of a wavelength. However, in tissue, small scatterers at the cellular level and microstructural level such as the arterioles and capillaries will have a dimensions on the order of 10 microns, much smaller than typical pulse shapes (the wavelength at 10 MHz is 150 microns, for example, and the

pulse length will be multiples of this). With many subresolvable scatterers interacting with a propagating pulse, the resulting echo will exhibit the random constructive and destructive interference pattern known as speckle (Burckhardt, 1970; George and Jain, 1973; George *et al.*, 1976; Burckhardt, 1978; Wagner *et al.*, 1983; Tuthill *et al.*, 1988; Reynolds *et al.*, 1989). The problems with a visual interpretation of speckle images are profound because the patterns of nulls and peaks may or may not correspond to actual nulls or peaks of the scatterers but rather to their summation over the positive and negative portions of the propagating pulse. Furthermore, the lesion detection problem is made more difficult by the overlap of Rayleigh statistics from different distributions of a lesion and a background (Sperry and Parker, 1991; Cramblitt and Parker, 1999). Attempts to improve the situation include speckle reduction algorithms (Bamber, 1993) and deconvolution approaches (Jensen, 1992; Alam *et al.*, 1998; Haider *et al.*, 1998; Taxt and Frolova, 1999; Qinzhen *et al.*, 2003; Michailovich and Adam, 2004; Kerner and Porat, 2008; Shin *et al.*, 2010). Despite all these attempts, the typical medical ultrasound image still retains the two characteristic elements of: resolution limited by the pulse size and shape and speckle statistics. There are reasons to suspect that this is an intractable problem. The spectrum of a typical pulse is a band-pass signal, so the dc, very low frequency, and very high frequency components of the reflectors are not captured. This limits the amount of “whitening” or equalization that can be accomplished. From a 2D imaging point of view, the illumination of k-space by a typical pulse is a discouragingly small area of support, constraining the strategies for improving image quality while reducing speckle (Munson and Sanz, 1984).

This paper will demonstrate an approach to an inverse filter solution with stabilized ultrasound pulses. Stabilized

^{a)}Author to whom correspondence should be addressed. Electronic mail: kevin.parker@rochester.edu

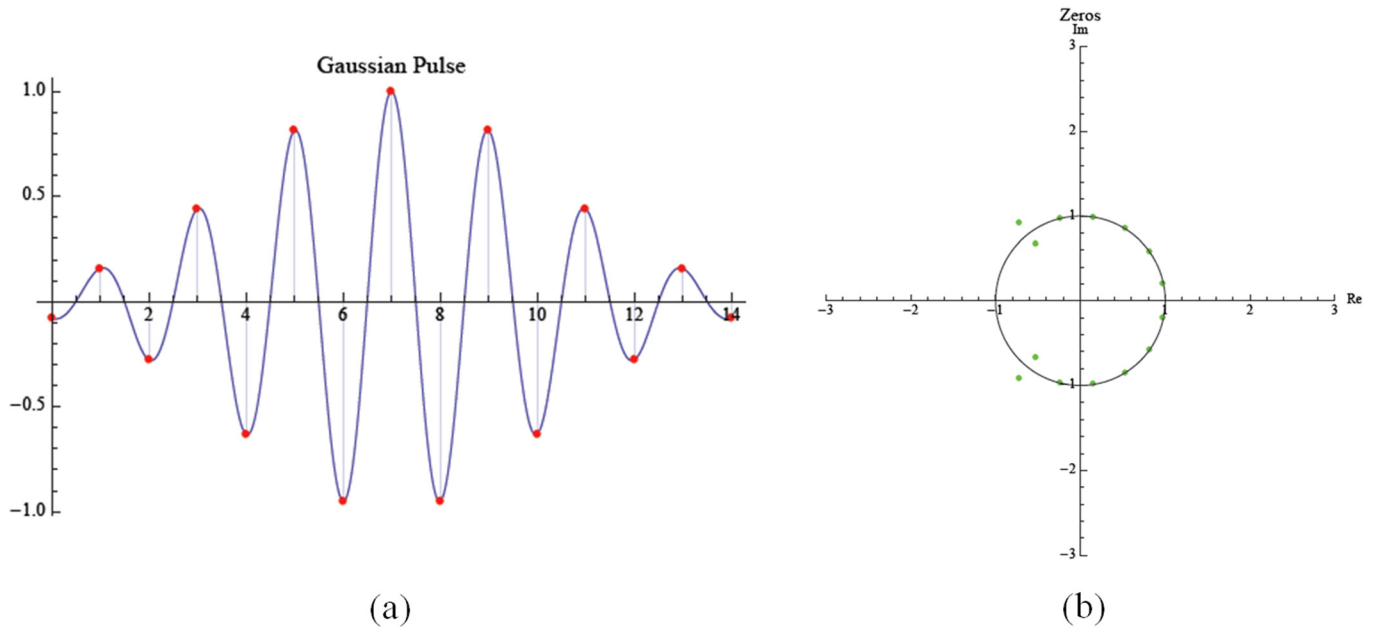


FIG. 1. (Color online) A conventional pulse with a Gaussian envelope, sampled at twice the center frequency in (a). The zeros of the Z-transform of the sampled pulse is shown in (b). Because some zeros lie in and around the unit circle, the inverse is unstable and unbounded.

pulses, in this context, mean realizable continuous functions in the axial and transverse directions that when sampled have their Z-transform zeros lying within the unit circle. This corresponds to inverse filters that are stable because their poles lie within the unit circle such that they are limited in time with bounded output. By applying an exact, stable inverse filter, the final result is a very high resolution, subwavelength solution to the distribution of scatterers that were previously below the resolution of the ultrasound pulse and the imaging system. The integration of random scatterers over the pulse length and width is essentially disaggregated by the inverse

filter operation. Therefore, the two dominant and problematic system effects of pulse length and speckle statistics are eliminated, replaced by a more favorable and high resolution calculation of the distribution of scatterers within tissue. The solution is exact within the framework of the convolution model and sampled signals, yet is approximate in the sense that the sampling frequency (as low as twice the center frequency of the transmit pulse in some following examples) will result in aliasing of components above the Nyquist frequency. The solutions are also accurate with respect to the physical reality to the extent that the convolution model is

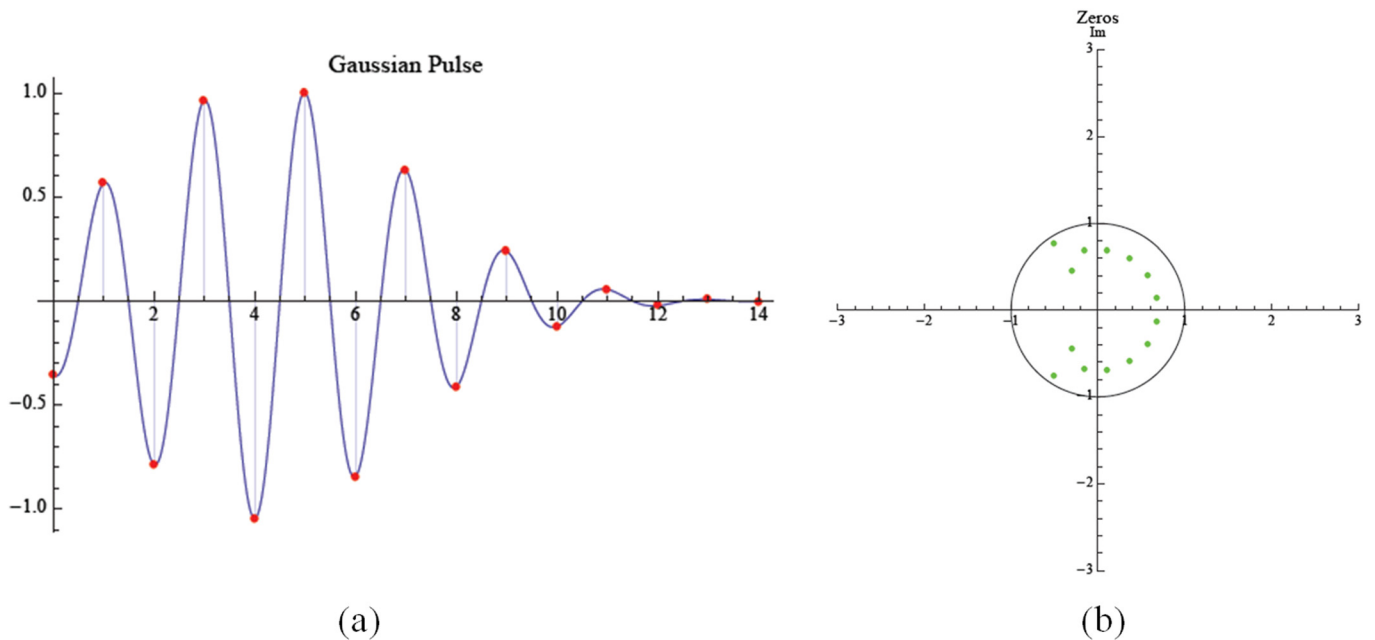


FIG. 2. (Color online) An asymmetric pulse formed by multiplying the Gaussian envelope with a geometric series is shown in (a). The zeros of the Z-transform are retracted into the unit circle as shown in (b). This leads to a stable inverse filter.

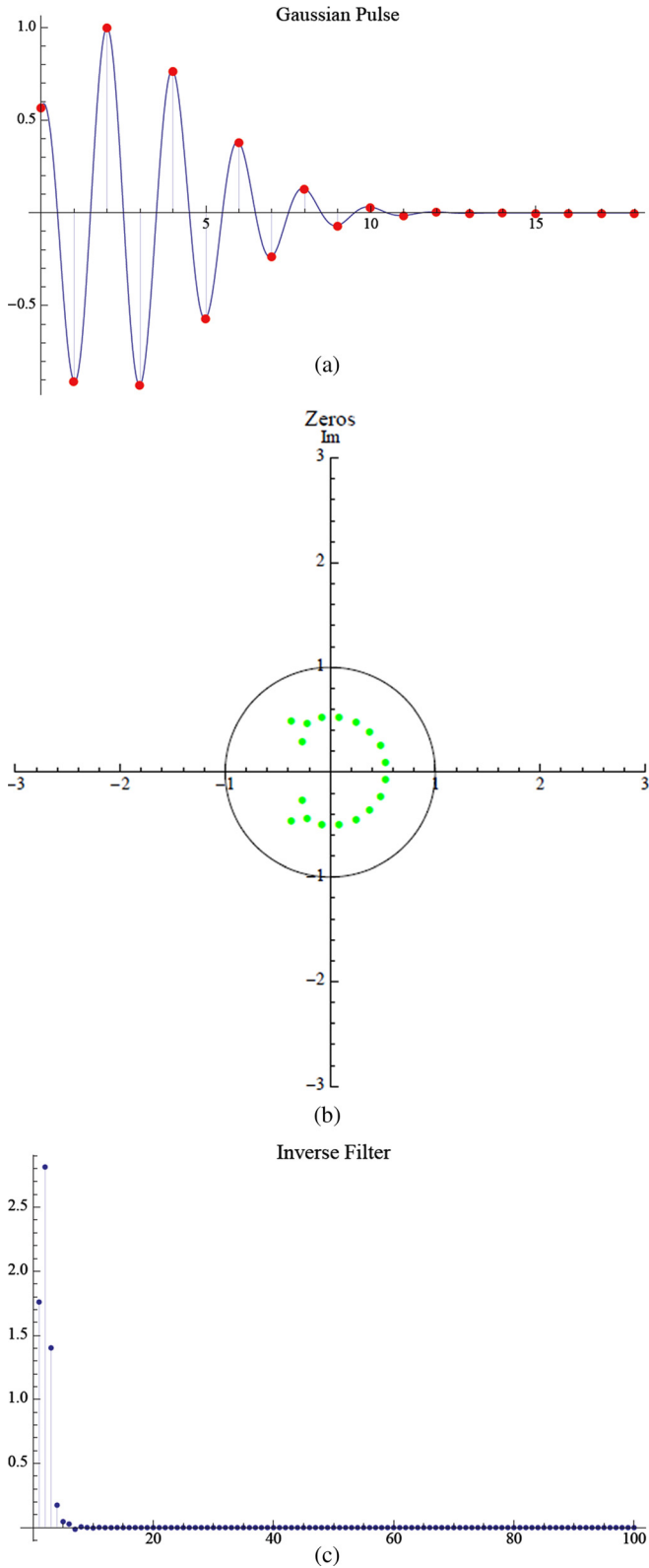


FIG. 3. (Color online) Another asymmetric pulse with the form of a Gaussian multiplied by the square root of t is shown in (a). The zeros of its Z-transform are shown in (b) indicating the availability of a stable inverse filter shown in (c).

accurate and the effect of noise is limited. The resulting images are termed super-resolution ultrasound (SURUS) images, as they are super-resolution ultrasound images.

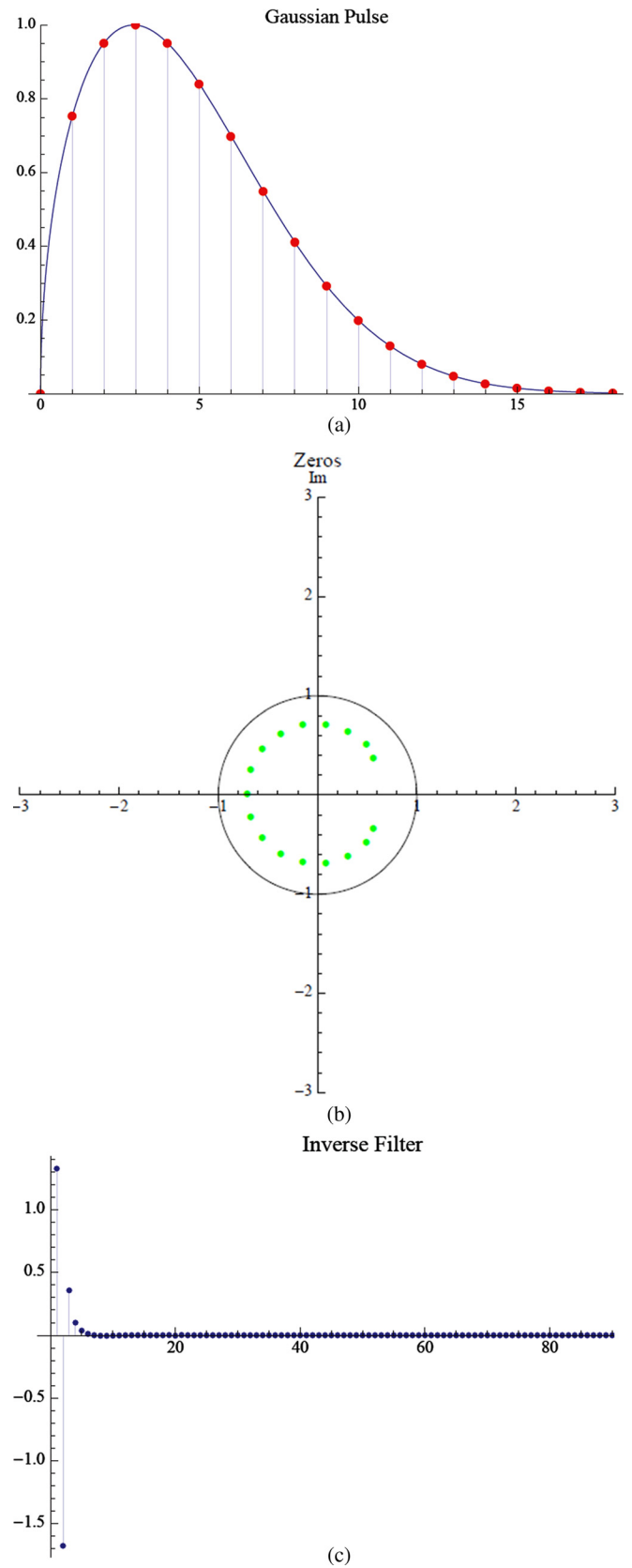


FIG. 4. (Color online) An unmodulated asymmetric envelope proposed for the transverse beam pattern is shown in (a). Its Z-transform zeros are shown in (b) and corresponding stable inverse filter in (c).

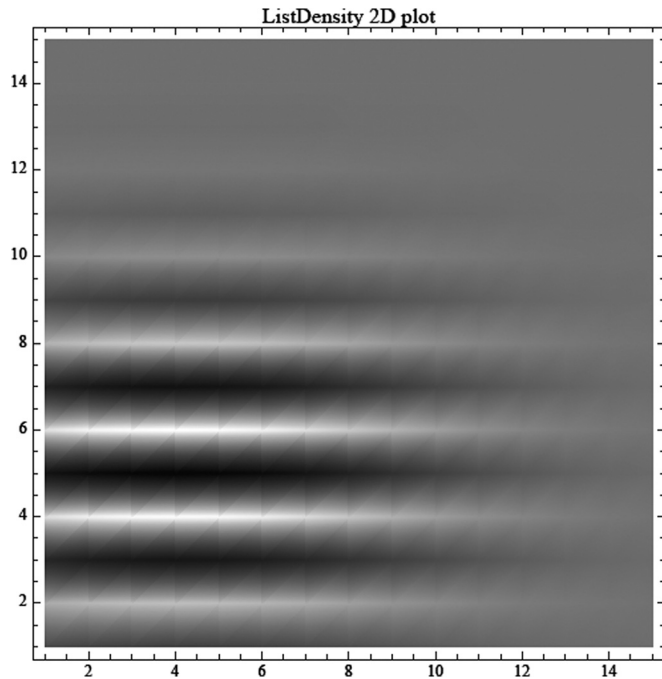


FIG. 5. A gray-scale plot of the two dimensional (2D) function that is separable and asymmetric in both vertical and horizontal directions. The vertical (axial) function is given by the function shown in Fig. 3(a), and the horizontal (transverse) function is the function shown in Fig. 4(a).

II. THEORY

We begin with a discrete version of Eq. (1) with the inclusion of noise. Without loss of generality, the 2D version is given as

$$e[n] = p[n]s[m] ** R[n, m] + g[n, m] \quad (2)$$

where $g[n, m]$ is additive noise.

The objective is to reconstruct the scatterers or reflectors $R[n, m]$. For this, we turn to the Z-transform of $p[n]$. The one-sided Z-transform of $p[n]$ is given by (Oppenheim and Schafer, 1975)

$$P(z) = \sum_0^{\infty} p[n]z^{-n}. \quad (3)$$

For a pulse of length N , the Z-transform is a polynomial of order $N-1$, which can be factored into roots, giving zeros of the Z-transform. The inverse filter, given by the transform $1/P(z)$, will convolve with $p[n]$ to produce an impulse. However, it is clear that the reciprocal nature of $P(z)$ and its inverse filter transform implies that the zeros of the pulse transform $P(z)$ become the poles of the inverse filter. Generally, for a casual, right-handed system to be stable the poles of the Z-transform must lie within the unit circle, and the region of convergence includes the unit circle. This is analogous to poles of a stable system lying in the left half plane

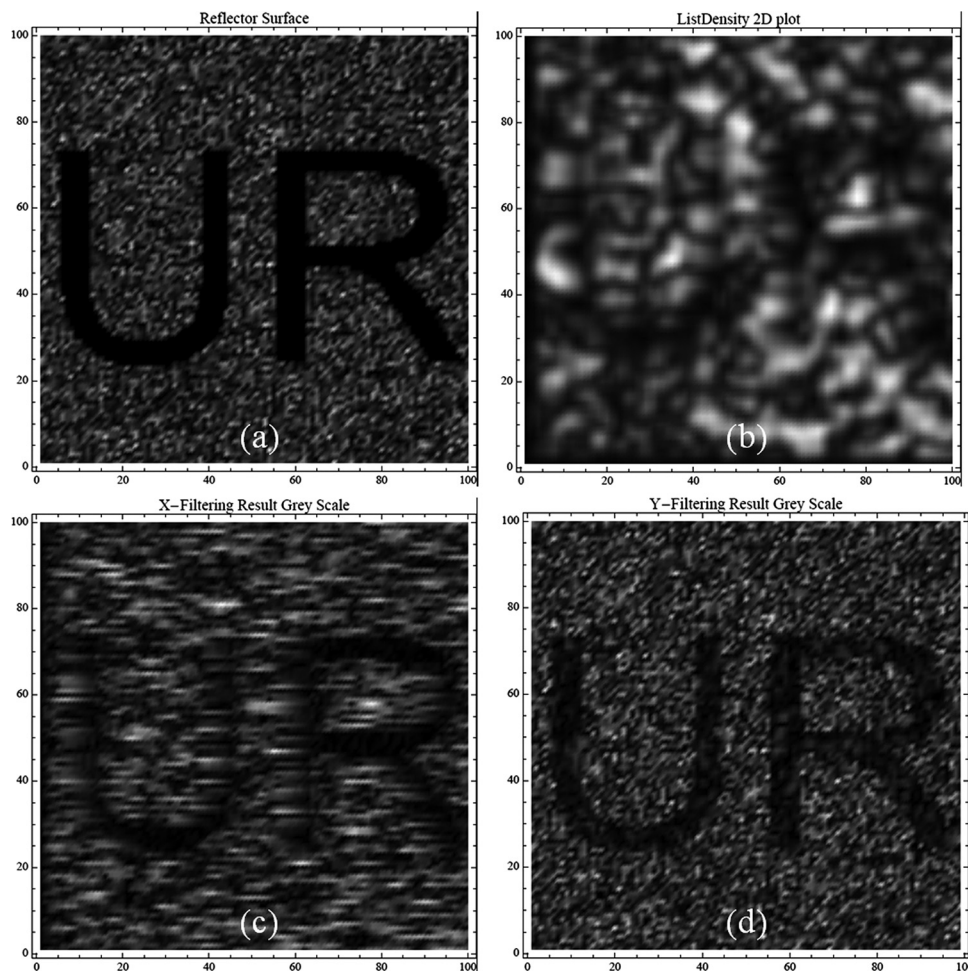


FIG. 6. A set of random reflectors with patches of zeros in the shape of letters (a) undergoes 2D convolution with the pulse of Fig. 5. The resulting speckle envelope is shown in (b), and the letters “UR” are not visible due to the distribution of the speckle statistics. After inverse filtering in the vertical direction, the results are improved in (c), and after horizontal inverse filtering the final result is given in (d); 5% rms white noise was added to the convolution result before inverse filtering, so the operations are well conditioned in the presence of modest additive noise.

for Laplace transforms. With poles on or outside the unit circle, the impulse response of these systems would be unstable and unbounded.

Assuming that a stable inverse filter $1/P(z)$ can be derived, with an impulse response of $p^{-1}[n]$, then a convolution of the received echo with the inverse filter yields

$$p^{-1}[n] * e[n] = p^{-1}[n] * p[n] * R[n] + p^{-1}[n] * g[n] \quad (4)$$

where the one-dimensional form of Eq. (2) is used for simplicity. Also, by definition

$$p^{-1}[n] * p[n] = \delta[n], \text{ the discrete delta function, so} \quad (5)$$

$$\begin{aligned} p^{-1}[n] * e[n] &= \delta[n] * R[n] + p^{-1}[n] * g[n] \\ &= R[n] + p^{-1}[n] * g[n]. \end{aligned} \quad (6)$$

In the absence of noise, the use of the inverse filter yields $R[n]$ exactly, a high resolution replica of the sampled scatter function. Given noise, the stability and frequency response of $p^{-1}[n]$ must be considered to minimize the term $p^{-1}[n] * g[n]$.

Thus far we considered the general case of a one-dimensional signal $p[n]$ and its Z-transform. Because our imaging pulse is two (or three) dimensional, we need to consider a two (or three) dimensional Z-transform. However, because the convolutional model has separable functions for axial and transverse dimensions, then the 2D Z-transform reduces to separable functions as well.

The problem, therefore, is to find and apply inverse filters for $p[n]$ and $s[m]$. Unfortunately, the typical ultrasound pulses used for imaging are functions that, when sampled, have Z-transforms with many zeros on and outside of the unit circle [see Michailovich and Adam (2004) for examples]. These produce inverse filters with poles outside of the unit circle, leading to unstable filters. Further examples are given in Sec. III.

One way to create stabilized pulses (meaning pulses that, when sampled, possess stable inverse filters) is to multiply $p[n]$ by the quantity β^n , where β is a real number < 1 . In the discrete world, if a right-sided sequence $p[n]$ with a Z-transform $P(Z)$ is multiplied by an exponential sequence β^n , then (Oppenheim and Schaffer, 1975; Jackson, 1991)

$$Z[\beta^n p[n]] = P(z/\beta). \quad (7)$$

Thus the multiplication by a geometric series creates an asymmetric pulse in the time domain with its Z-transform zeros “retracted” into the unit circle depending on the factor beta. A similar consideration applies to samples of the transverse beam function $s[m]$, and examples are provided in the next section.

III. RESULTS

First, we examine a conventional pulse shape $p[n]$, which is modeled as a Gaussian envelope modulated by a cosine at the center frequency of the transducer as shown in Fig. 1(a). The continuous function is sampled at twice the center

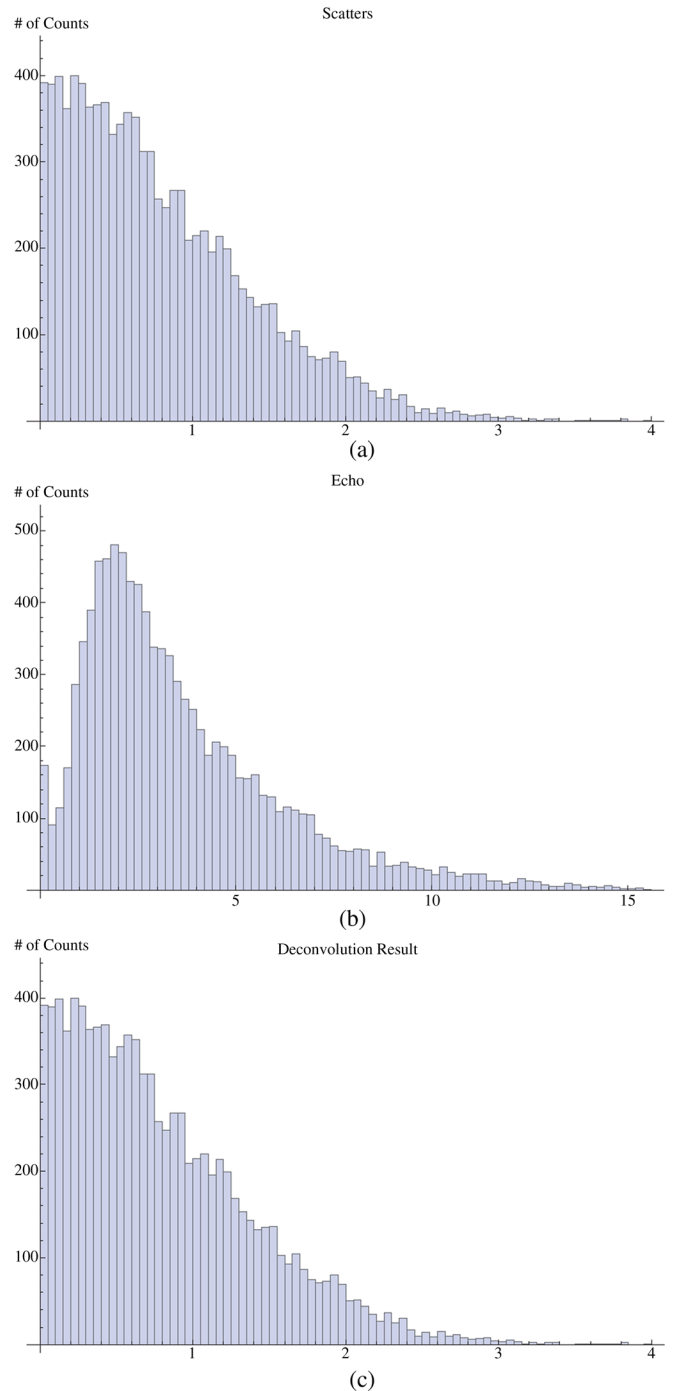


FIG. 7. (Color online) Histograms showing the probability density functions for the original scatters (a), the result of convolution with a pulse (b), and after inverse filtering (c). The standard Rayleigh speckle statistics are demonstrated in (b), whereas the original Gaussian statistics are restored in (c).

frequency and 15 points are taken as $p[n]$. The Z-transform of this sampled pulse has numerous zeros on the unit circle and a pair of conjugate zeros outside of the unit circle, as seen in Fig. 1(b).

These zeros will become poles of the inverse filter and signify an unstable, unbounded output result. Therefore this class of typical pulse echo shape is not conducive to inverse filters. However, by modifying the function with a geometric series, a beta term in Eq. (7), the pulse can be made asymmetric and the inverse transform is stabilized. As an

example, the Gaussian function in Fig. 1(a) is multiplied by 0.7^n , and the new function is shown in Fig. 2(a).

Now all the zeros of the transform lie within the unit circle, as seen in Fig. 2(b). Accordingly, the inverse filter will have poles within the unit circle and will have a bounded input/bounded output impulse response of limited duration.

In general, we have found that the formation of a stabilized pulse is not restricted to the use of a β^n type function; rather this is illustrative of envelopes that have a sharp initial rise and a more gradual fall-off from the peak. We call these “asymmetric” envelopes or pulses, and these can be characterized by a number of different analytic functions. One example is a piecewise exponential rise with one time constant and then an exponential fall with a longer time constant. Another example for a pulse is a Gaussian function in time multiplied by a sine or cosine, as in conventional modulation, but with a step function at $t = 0$ and multiplied by t ,

$$p(t) = \sin(\omega t + \varphi) * \sqrt{t} * e^{-(t-\tau)^2/2\sigma^2} * \text{UnitStep}(t). \quad (8)$$

This produces an asymmetric envelope similar to a Rayleigh distribution function. When sampled at twice the modulation frequency and aligned to the peaks of the function, the resulting sampled $p[n]$, and its pole-zero diagram and its inverse filter are shown in Fig. 3.

For the transverse beam pattern $s(x)$, we choose the asymmetric function:

$$s(x) = x * e^{[-x^2/2\sigma_x^2]} * \text{UnitStep}(x). \quad (9)$$

The sampled version, $s[m]$ is given in Fig. 4, along with the corresponding pole-zero diagram and the inverse filter result. The rapid decay of this inverse filter, along with the inverse of $p[n]$, is quite beneficial to the suppression of noise.

The combined pulse $p[n]s[m]$ in two dimensions is shown in Fig. 5, and its non-symmetry is readily apparent.

This pulse is used to image a field of random scatterers, with a pattern of letter-shaped nulls running through the field [Fig. 6(a)]. The 2D pulse shape is approximately 12 samples (vertical, axial) by 15 samples (horizontal, transverse) and will at any position include approximately 180 sampled scatterers, resulting in fully developed speckle. The conventional speckle pattern results [Fig. 6(b)] and the null characters cannot be discerned. After convolution with axial (vertical) and transverse (horizontal) inverse filters, the original pattern is reproduced exactly except for the effects of 5% rms noise added to the original signal before inverse filtering [Figs. 6(c) and 6(d)]. In this example, the improvement in resolution compared with conventional pulse echo is approximately a factor of 12 in the axial and 15 in the transverse dimensions.

From the visual appearance, the speckle pattern has been converted to a fine-grain scatterer map. Statistically, the unfavorable Rayleigh statistics of speckle are converted into the statistics of the original scatterers. This is demonstrated in Fig. 7. Plotted are the histograms of the absolute value of the original scatterers (a), the envelope of the echo demonstrating Rayleigh statistics (b), and the absolute value of the echo after filtering (c). The original Gaussian distribution of the scatterers has been restored.

The effect of sampling rate is important, and a general trend is illustrated in the following example. A pulse shape of the form of Eq. (8) is sampled at exactly twice the modulation frequency in Fig. 8 along with its pole-zero diagram, which indicates the availability of a stable and useful inverse filter.

If the sampling rate is doubled as shown in Fig. 9(a), the length of the sampled pulse doubles (increasing the complexity of the solution for the zeros of the Z-transform and then the inverse Z-transform), and the pole-zero diagram [Fig. 9(b)] demonstrates a similar pattern to the previous

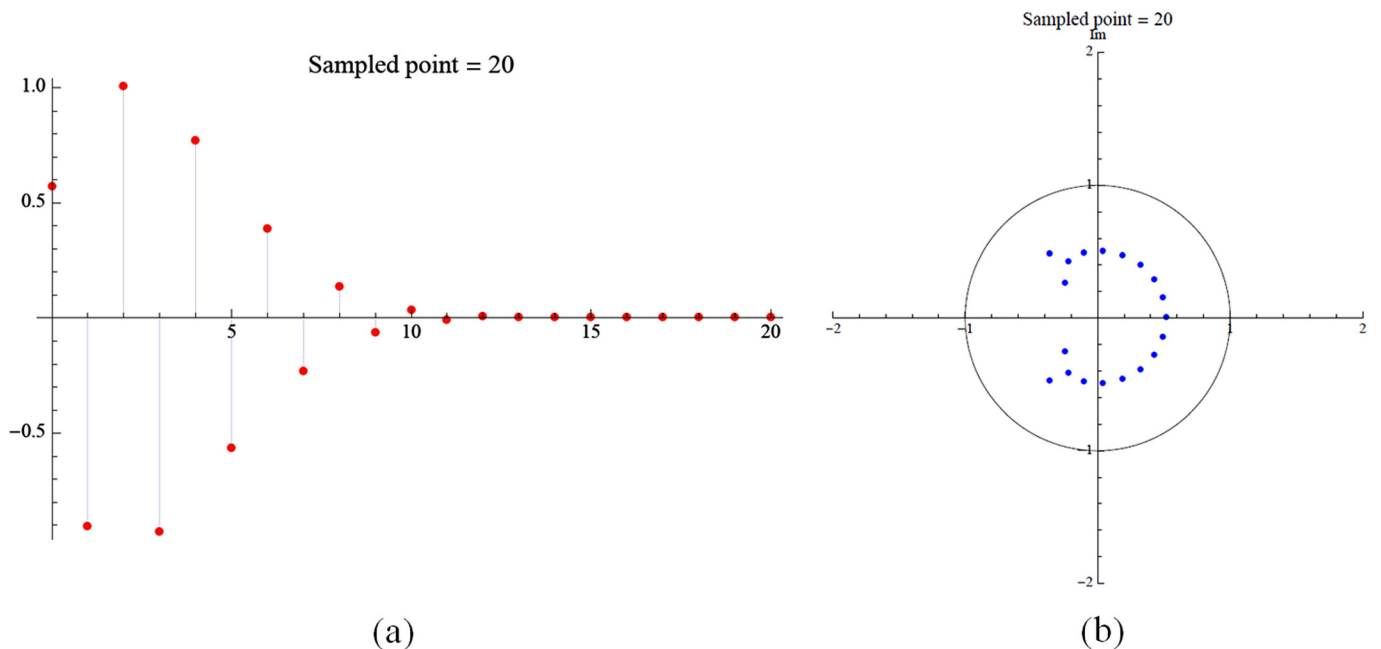


FIG. 8. (Color online) A sampled pulse (a) and its Z-transform zeros (b) indicating the availability of a stable inverse filter.

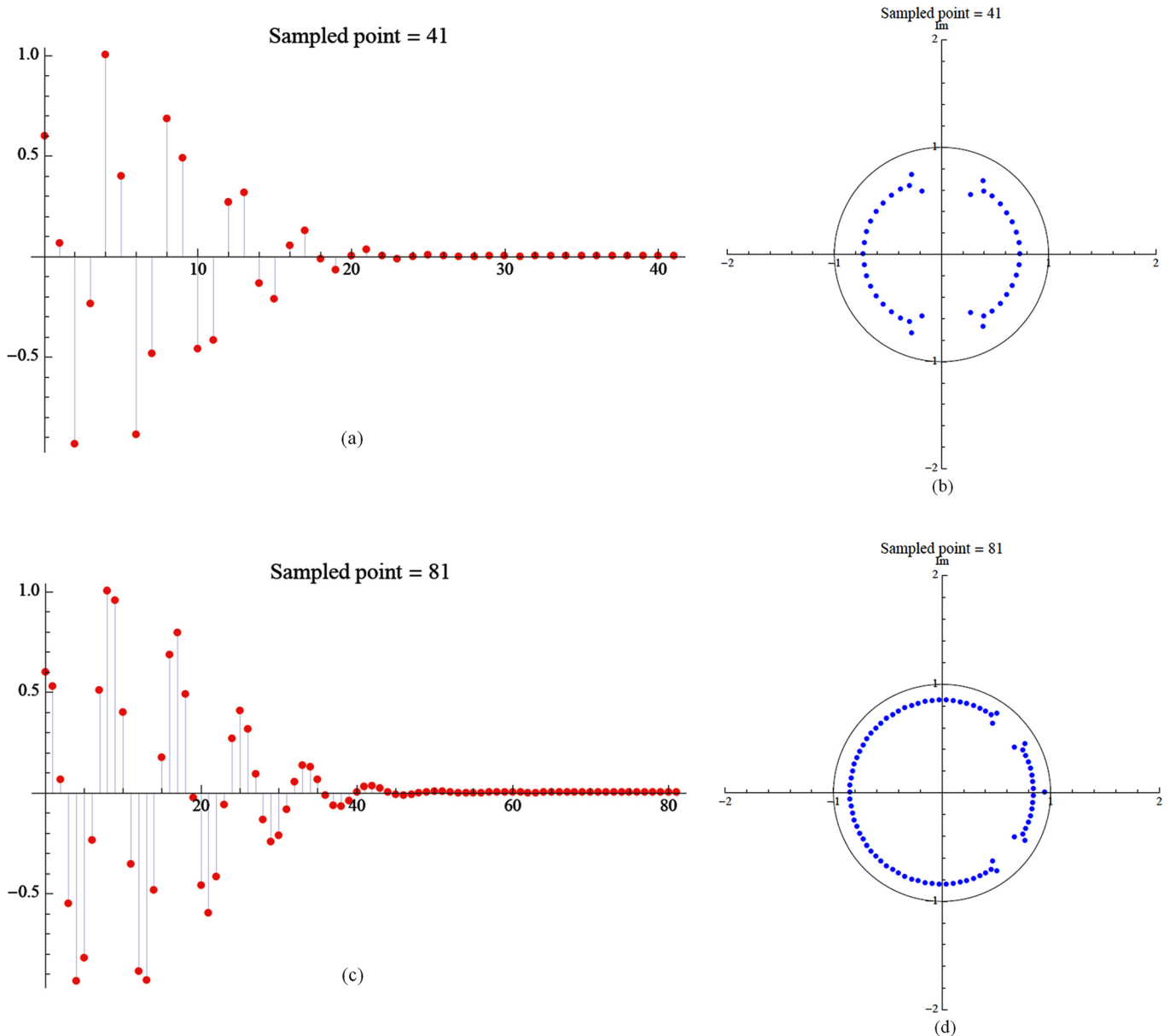


FIG. 9. (Color online) The same pulse sampled at twice the sampling rate of Fig. 8, shown in (a), and its Z-transform zeros in (b). A movement toward the unit circle is evident. Another doubling of the sampling rate results in (c) and (d). The trend is toward the unit circle and instability.

example but with double the number of zeros and a shift toward the unit circle.

Continuing along this direction, if we again double the sampling frequency [Fig. 9(c)], then the poles double and once again trend toward the unit circle [Fig. 9(d)].

The closest points to the unit circles will correspond to peaks in the frequency response of the inverse filter, producing ringing, poor convergence, and in the limit, instability. Thus, even within the convolution model framework, there is a limit to the degree of superresolution that is achievable with a given asymmetric pulse.

Another issue concerns the sensitivity of the superresolution result to the exact parameters. In practice, even with a well designed transmit pulse and beam, inhomogeneities and fluctuations within the tissue will create distortions in the propagating pulse. So a reconstruction that requires exact parameters would be limited in value. To test this, a convolu-

tion with a pulse is performed using one pulse shape and then is inverse filtered using a different parameter. The pulse $p[t]$ was chosen to be of the form of a Gaussian modulated cosine multiplied by a β^t where $\beta = 0.7$. The inverse filter for this was calculated assuming an incorrect β of 0.6, other parameters and transverse beam pattern remaining the same. The original scatterers, speckle image, deconvolution in the vertical direction, then full vertical and horizontal directions are given in Fig. 10. While the inverse filter result is no longer a close match to the original scatterer pattern, the UR-shaped voids can still be seen, thus a degree of superresolution is achieved without the use of exact parameters.

IV. DISCUSSION AND CONCLUSIONS

An inverse filter approach has been derived using the Z-transform on stabilized but realizable pulses. Analogous

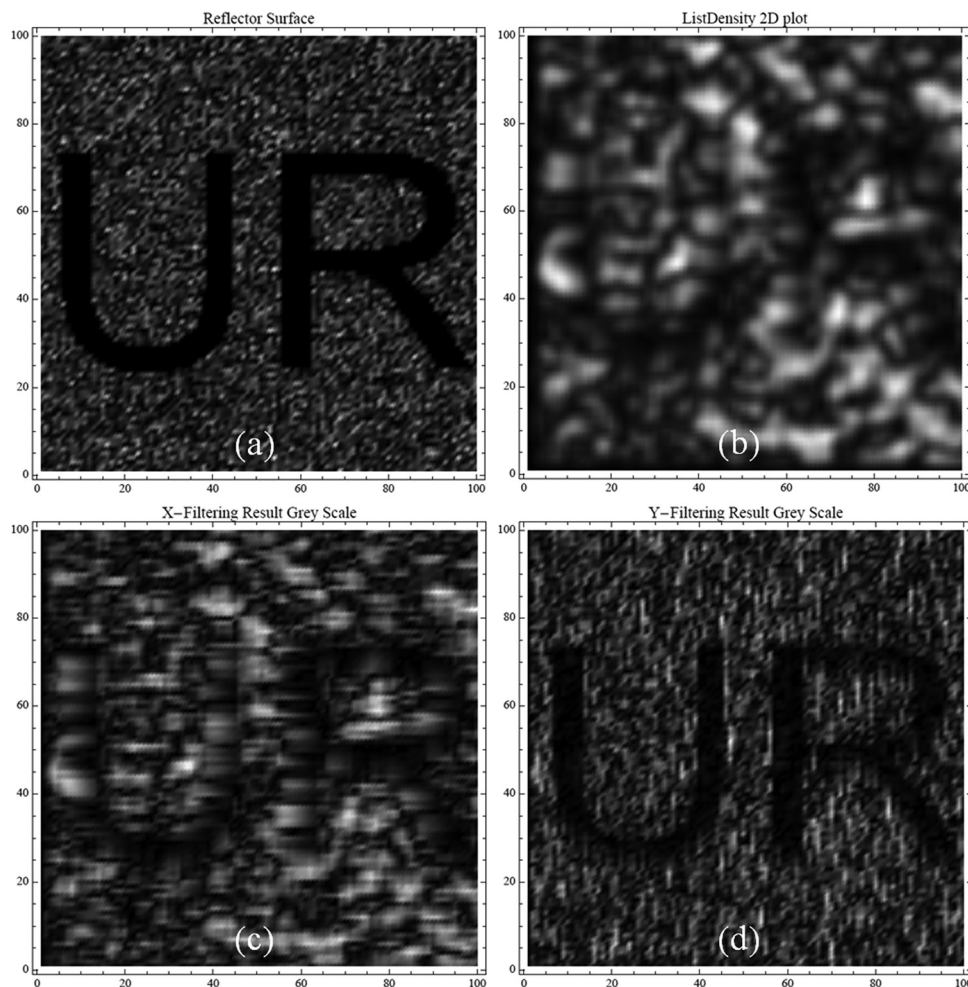


FIG. 10. The effect of inexact reconstruction parameters. A region of reflectors is shown in (a). Imaging with a pulse using a geometric parameter of 0.7 yields a conventional speckle image in (b). Reconstruction with horizontal (exact) and vertical (inexact, geometric parameter 0.6 used) are shown in (c) and (d), respectively. The resulting inverse filtered image is a reasonable reconstruction of the original scatterers, despite the use of an erroneous model.

inverse filters may be derived using alternative approaches (Fourier transform, Chirp-Z transform, and others), and other functions besides β^t can be utilized to produce stabilized yet practicable pulse shapes. However, the use of the Z-transform and the effect of the beta function in the transform domain are fundamental and illustrative.

A major issue in the use of the inverse filter is the limit of accuracy of the framework. There are a number of contributing factors. The first is the accuracy of the convolutional model compared to the physical world. In particular, the separability of the pulse function into axial and transverse functions is well accepted for the focal region but not in the near field. However, the increasing use of multiple focus zones and dynamic focus adjustments in imaging systems means that more zones within the image are likely to be represented by a separable function. In the event that the pulse cannot be decomposed into separable functions, a 2D Z-transform can still be applied. Given a 2D pulse function $p[n, m]$ with its 2D Z-transform $P[z_1, z_2]$, it can be shown that the asymmetric principle applies in 2D. That is, $a^n \cdot b^m \cdot p[n, m]$ has the transform $P[z_1/a, z_2/b]$ (Oppenheim and Schaffer, 1975). Thus proper asymmetric shaping of the pulse can be used in both axial and transverse directions to “retract” the zeros into the unit sphere in 2D for stability of the 2D inverse filter. In practice, the difficulties caused by inhomogeneous overlying tissues and attenuation will cause

the true pulse shape to deviate from the ideal. The results of Fig. 10 demonstrate that there can be some improved resolution with this approach even when a model parameter is off by over 10%. It remains to be seen how well the parameters can be adjusted to account for tissue distortion over a range of patients and organs.

A second issue is that of noise because the inverse filter convolves with the additive noise to produce an unwanted term. For inverse filters with poles very close to or on the unit circle, there can be an amplification of the noise near the pole frequencies. Thus the design of the inverse filter and limiting or suppression of noise are important issues. A third factor is the sampling rate, which in a naive view could be set very high leading to arbitrarily fine resolution. This scheme is not practical because higher sampling rates lead to larger polynomials in the Z-transform, more difficult solutions of the polynomial roots and inverses, and more poles in the inverse filter, which will become more difficult to constrain within the unit circle. Thus a practical upper limit will be reached; however, the details are beyond the scope of this paper.

Can these asymmetric pulses be produced in practice? In fact it is straightforward to show that the Fourier transform of the conventional symmetric beamshapes, and those of the asymmetric versions, are reasonably contained within a similar support or bandwidth. That means that a transducer of limited bandwidth can, with some modification of the

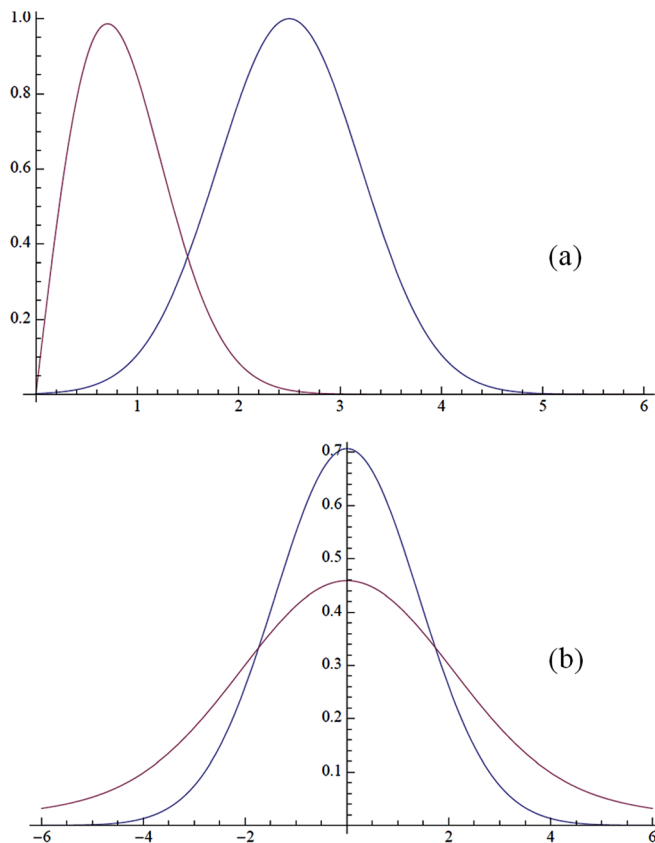


FIG. 11. (Color online) Two functions in the spatial domain, a Rayleigh and a Gaussian, representing asymmetric and symmetric pulse envelopes, are given in (a). Their Fourier Transform magnitudes are given in (b). A somewhat greater distribution of the higher spatial frequencies is required to generate an asymmetric beam envelope.

excitation, produce either the symmetric or the asymmetric (stabilized) version of $p(t)$. For the transverse beam pattern, this means that an aperture with limited support can similarly produce either the symmetric or the asymmetric (stabilized) version of the beam pattern $s(x)$. As an example, consider two functions of x , one a standard Gaussian and the other of the form x times a Gaussian, as shown in Fig. 11(a). One is clearly asymmetric, leading to a stable inverse filter. The magnitude of the Fourier transform of both functions is shown in Fig. 11(b). The asymmetric function, being more narrow in the x domain, has a greater bandwidth in the transform domain. An imaging system would require a somewhat broader aperture or transducer excitation to achieve the asymmetric function in the lateral or axial dimensions, respectively. Thus there is some cost associated with realizing pulse shapes that are opportune for inverse filtering and superresolution.

The result of employing stabilized pulses and their inverse filters is highly beneficial for the imaging of small reflectors or scatterers, and for low-contrast lesion detection in B-scan imaging systems, because the dominant and problematic characteristics of resolution linked to pulse length, and speckle statistics, are eliminated. Instead, resolution is linked to the sampling frequency: for example twice the center frequency of the transducer, leading to an improvement of at least 6–10 in typical broadband system resolution, more for narrowband systems. Furthermore, the statistics of the so-

lution to the inverse filter resemble the statistics of the actual scatterer distribution as sampled at the desired sampling frequency. This approach is tractable, can be implemented on most scanning systems, and is adaptable to a wide variety of specific transducers, bandwidths, and applications. Similar considerations apply to other imaging schemes that employ coherent pulses, including OCT systems, and some sonar, radar, and SAR pulse-echo systems.

ACKNOWLEDGMENTS

This work was supported by the Department of Electrical and Computer Engineering in the Hajim School of Engineering of the University of Rochester. The author is grateful to Zhilin (Aaron) Cong who produced superb programs for solving and incorporating inverse Z-transforms.

- Alam, S. K., Ophir, J., Cespedes, I., and Varghese T. (1998). "A deconvolution filter for improvement of time-delay estimation in elastography," *IEEE Trans. Ultrason. Ferroelectr. Freq. Control* **45**, 1565–1572.
- Bamber, J. C. (1993). "Speckle reduction," in *Advances in Ultrasound Techniques and Instrumentation* (Churchill Livingstone, New York), pp. 55–67.
- Burckhardt, C. B. (1970). "Laser speckle pattern—a narrowband noise model," *Bell Syst. Tech. J.* **49**, 309–316.
- Burckhardt, C. B. (1978). "Speckle in ultrasound B-mode scans," *IEEE Trans. Ultrason. Ferroelectr.* **25**, 1–6.
- Cramblitt, R. M., and Parker, K. J. (1999). "Generation of non-Rayleigh speckle distributions using marked regularity models," *IEEE Trans. Ultrason. Ferroelectr. Freq. Control* **46**, 867–874.
- George, N., Christensen, C. R., Bennett, J. S., and Guenther, B. D. (1976). "Speckle noise in displays," *J. Opt. Soc. Am.* **66**, 1282–1290.
- George, N., and Jain A. (1973). "Speckle reduction using multiple tones of illumination," *Appl. Opt.* **12**, 1202–1212.
- Haider, B., Lewin, P. A., and Thomenius, K. E. (1998). "Pulse elongation and deconvolution filtering for medical ultrasonic imaging," *IEEE Trans. Ultrason. Ferroelectr. Freq. Control* **45**, 98–113.
- Jackson, L. B. (1991). "Signals, systems, and transforms," in *Addison-Wesley Series in Electrical Engineering* (Addison-Wesley, Reading, MA), pp. 59–136.
- Jensen, J. A. (1992). "Deconvolution of ultrasound images," *Ultrason. Imaging* **14**, 1–15.
- Kerner, Y., and Porat, M. (2008). "Acoustic imaging using a maximum likelihood approach," in *Direct and Inverse Problems of Electromagnetic and Acoustic Wave Theory (2008)*. DIPED 2008 13th International Seminar/Workshop, pp. 163–167.
- Macovski, A. (1983). "Basic ultrasonic imaging," in *Medical Imaging Systems* (Prentice-Hall, Englewood Cliffs, NJ), pp. 173–203.
- Michailovich, O., and Adam, D. (2004). "Phase unwrapping for 2-D blind deconvolution of ultrasound images," *IEEE Trans. Med. Imaging* **23**, 7–25.
- Munson, D. C., and Sanz, J. L. C. (1984). "Image-reconstruction from frequency-offset Fourier data." *Proc. IEEE* **72**, 661–669.
- Oppenheim, A. V., and Schaffer, R. W. (1975). *Digital Signal Processing* (Prentice-Hall, Englewood Cliffs, NJ), Chap. 2, pp. 45–86.
- Prince, J. L., and Links, J. M. (2006). "Ultrasound imaging systems," in *Medical Imaging Signals and Systems* (Pearson Prentice-Hall, Upper Saddle River, NJ), pp. 347–78.
- Qinzheng, X., Suiwen, W., Wenjiang, P., and Luxi, Y. (2003). "Ultrasonic image processing using wavelet based deconvolution," in *Proceedings of the 2003 International Conference on Neural Networks and Signal Processing*, Vol. 2, pp. 1013–1016.
- Reynolds, G. O., DeVelis, J. B., Parrent, G. B., and Thompson, B. J. (1989). "Sources of coherent noise and their reduction," in *The New Physical Optics Notebook: Tutorials in Fourier Optics* (AIP, New York), pp. 199–219.
- Shin, H. C., Prager, R., Gomersall, H., Kingsbury, N., Treece, G., and Gee, A. (2010). "Estimation of average speed of sound using deconvolution of medical ultrasound data," *Ultrasound Med. Biol.* **36**, 623–636.
- Sperry, R. H., and Parker, K. J. (1991). "Segmentation of speckle images based on level-crossing statistics," *J. Opt. Soc. Am. A* **8**, 490–498.

- Szabo, T. L. (2004). "Wave scattering and imaging," in *Diagnostic Ultrasound Imaging: Inside Out* (Elsevier Academic, Amsterdam), pp. 213–242.
- Taxt, T., and Frolova, G. V. (1999). "Noise robust one-dimensional blind deconvolution of medical ultrasound images," *IEEE Trans. Ultrason. Ferroelectr. Freq. Control* **46**, 291–299.
- Tuthill, T. A., Sperry, R. H., and Parker, K. J. (1988). "Deviations from Rayleigh statistics in ultrasonic speckle," *Ultrason. Imaging* **10**, 81–89.
- Wagner, R. F., Smith, S. W., Sandrik, J. M., and Lopez, H. (1983). "Statistics of speckle in ultrasound B-scans," *IEEE Trans. Sonics Ultrason.* **30**, 156–163.